FACULTY OF ELECTRICAL ENGINEERING
KTE
September 7. - 9.9.2009
Cheb, Czech Republic

STATIC CHARACTERISTICS OF COMPONENTS OF CONTROLLABLE THERMOELASTIC ACTUATOR

PROF. ING. IVO DOLEŽEL, CSC.
ING. VÁCLAV KOTLAN, PH.D.
DOC. ING. BOHUŠ ULRYCH, CSC.

Abstract: *The paper deals with one of the basic conditions of practical employment of finely controllable thermoelastic actuators – problems of the static characteristics of its individual structural parts. It contains the formulation of the principle of such thermoelastic actuators, description of its components (a dilatation element heated by induction, auxiliary electromagnetic actuators, and self-locking friction clutches) and their mathematical models. Briefly discussed are also their corresponding computer models making use of the finite element method. The crucial point of the work consists in the presentation of the results – static characteristics of the considered structural parts of the controlled thermoelastic actuators.*

Key words: *Electromagnetic field, temperature field, field of, thermoelastic displacements, electromagnetic actuator, self-locking friction clutch, controllable dilatation, finite element method.*

INTRODUCTION

The paper deals with specific devices for realization of extremely small (on the order of $10^{-6} - 10^{-3}$ m) controllable shifts. Such devices can be used in a number of technical domains such as

- *optics* – for example, setting of focal distances of lens systems,
- *laser technologies* – setting of position or focusing of the laser beam,
- *microscope technologies* – setting of the position of specimens with respect to the focus of light beams in case of optical microscopes or focus of a beam of electrons in case of electron microscopes, and
- *acceleration of charged particles* – setting of the position of a target with respect to a beam of accelerated particles.

For realization of devices generating extremely small, controlled shifts, we can use the phenomenon of the thermal dilatation. Such a device works on the principle of common uncontrolled thermoelastic actuators (see [1], [2]). This device is, moreover, supplemented with some auxiliary parts (friction clutch, miniature electromagnetic actuator and some others) allowing its accurate control.

A detailed description of such controllable thermoelastic actuators and qualitative evaluation of their practical technological employment is discussed in [3]. The presented paper deals with the quantitative static characteristics of the individual structural parts of these actuators that provide information necessary for their practical applications.

1 THE PROBLEM FORMULATION

The device represents a classical thermoelastic actuator [1], [2] that is supplemented by two miniature electromagnetic actuators supplied by pulse currents and two self-locking friction clutches controlled by these actuators. Its scheme is obvious from Fig. 1.

The harmonic current-carrying field coil **1** produces periodically varying magnetic field that generates eddy currents in the dilatation element **2** clamped in stiff wall (or flange) **4**. The hollow dilatation element contains thermal insulation **9** and working nonferromagnetic plunger **3** placed in two sliding bearings **7** and **8**. This plunger is controlled (fixed or released) by two conical self-locking friction clutches $\mathbf{S}_1$ (**5**) and $\mathbf{S}_2$ (**6**). These clutches are controlled by simple electromagnetic actuators $\mathbf{A}_1$ consisting of steel cylinders and coils $\mathbf{c}_{11}$, $\mathbf{c}_{12}$ and $\mathbf{A}_2$ containing analogous coils $\mathbf{c}_{21}$, $\mathbf{c}_{22}$. Operation of these auxiliary actuators $\mathbf{A}_1$, $\mathbf{A}_2$ and clutches $\mathbf{S}_1$, $\mathbf{S}_2$ is controlled by pulse currents introduced into the mentioned coils $\mathbf{c}_{11} - \mathbf{c}_{22}$. These pulse currents can be rela-

tively strong (but short) in order that the forces generated by these actuators and self-locking friction forces are sufficiently high, but without any danger of overheating the coils.

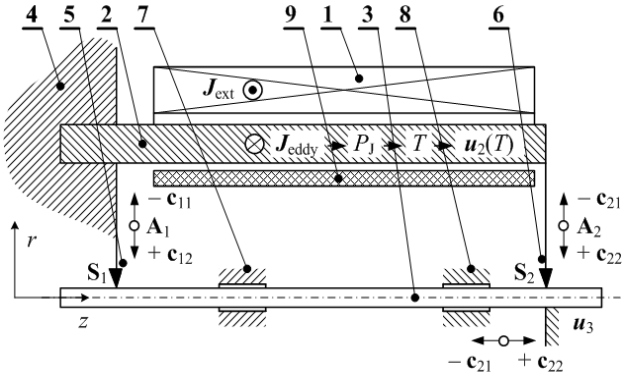

Fig. 1. Schematic arrangement of the controllable thermoelastic actuator:
1 *– field coil,* **2** *– dilatation element,* **3** *– nonferromagnetic plunger,* **4** *– stiff fixing wall (flange),* **5** *– self-locking friction clutch* $\mathbf{S}_1$ *controlled by actuator* $\mathbf{A}_1$*,* **6** *– other clutch* $\mathbf{S}_2$ *controlled by actuator* $\mathbf{A}_2$*,* **7***,* **8** *– sliding bearings,* **9** *– thermal insulation*

The detailed structural arrangement of the thermoelastic actuator with controllable working regime is shown in Fig. 2. The structures of the auxiliary electromagnetic actuators $\mathbf{A}_1$ and $\mathbf{A}_2$ is obvious from Figs. 3a and 3b and structures of self-locking friction clutches $\mathbf{S}_1$ and $\mathbf{S}_2$ in Figs. 4a and 4b.

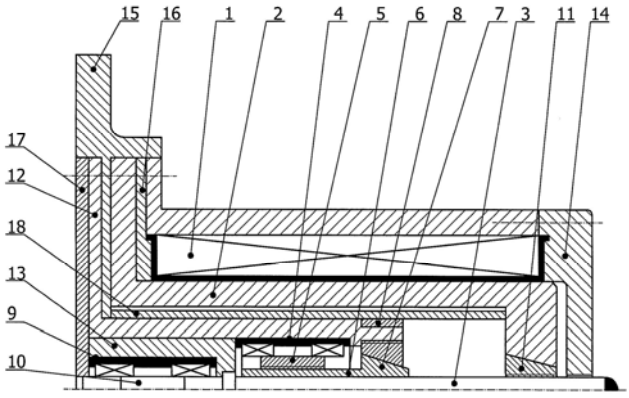

Fig. 2: Structural solution of the considered thermoelastic actuator:
1 *– field coil with its shell,* **2** *– dilatation element,* **3** *– nonmagnetic plunger,* **4***,* **5** *– electromagnetic actuator* $\mathbf{A}_1$ *of friction clutch* $\mathbf{S}_1$*,* **6***,* **7** *– friction clutch* $\mathbf{S}_1$*,* **8** *– fixing sleeve,* **9***,* **10** *– electromagnetic actuator* $\mathbf{A}_2$ *of friction clutch* $\mathbf{S}_2$*,* **11** *– friction clutch* $\mathbf{S}_2$*,* **12** *– case of actuator* $\mathbf{A}_1$*,* **13** *– case of actuator* $\mathbf{A}_2$*,* **14** *– external shell of the thermoelastic actuator,* **15** *– fixing flange,* **16** *– internal strap,* **17** *– external strap,* **18** *– thermoinsulation case*

The physical parameters of the individual structural parts of the thermoelastic actuator, as well as auxiliary electromagnetic actuators $\mathbf{A}_1$ and $\mathbf{A}_2$ and friction clutches $\mathbf{S}_1$ and $\mathbf{S}_2$ are listed in Tabs. 1–3.

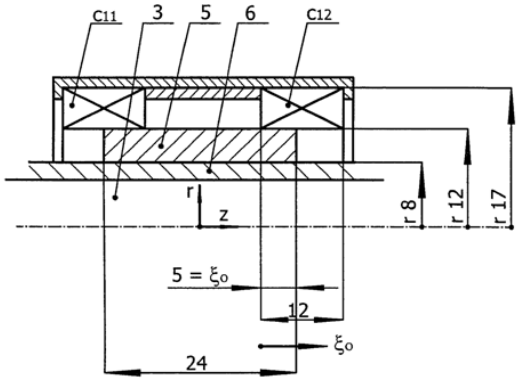

Fig. 3a: Arrangement of electromagnetic actuator $\mathbf{A}_1$*:* **5** *– ferromagnetic hollow core (connected with* **6***),* **6** *– nonferromagnetic body of friction clutch* $\mathbf{S}_1$*,* $\mathbf{c}_{11}$ *and* $\mathbf{c}_{12}$ *– field coils of the actuator*

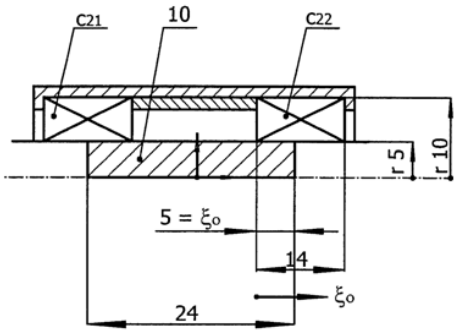

Fig. 3b: Arrangement of electromagnetic actuator $\mathbf{A}_2$*:* **10** *– ferromagnetic core (connected with* **3***),* $\mathbf{c}_{21}$ *and* $\mathbf{c}_{22}$ *– field coils of the actuator*

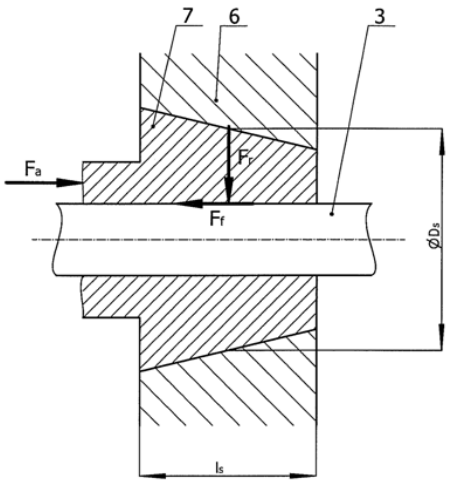

Fig. 4a: Friction clutch $\mathbf{S}_1$*:* **3** *– nonferromagnetic plunger of the thermoelastic actuator,* **6** *– conical sleeve of clutch* $\mathbf{S}_1$*,* **7** *– conical body of clutch* $\mathbf{S}_1$

We can distinguish three working regimes of the device, but they can easily be combined to obtain much more sophisticated operation processes:

- The clutch $\mathbf{S}_2$ is on, $\mathbf{S}_1$ is off: if the element **2** dilates, the plunger **3** shifts with it. If element **2** is in rest, so is the plunger.
- The clutch $\mathbf{S}_1$ is on, $\mathbf{S}_2$ is off: the plunger **3** is in the stable position even when the element **2** dilates or

shifts back in the process of cooling.

- Both clutches $\mathbf{S}_1$ and $\mathbf{S}_2$ are off and current pulses are transferred to both auxiliary coils $\mathbf{c}_{21}$ and $\mathbf{c}_{22}$. Thereby the plunger **3** is released and shifted to the starting position. Here it can be fixed by switching on the clutch $\mathbf{S}_1$.

Tab. 1: Physical parameters of the basic elements of the thermoelastic actuator (see Fig. 2)

	element	material	parameter	value	dim.
1	field coil	Cu conductor	diameter of conductor D_c	1	mm
			length of coil Δz	150	mm
			thickness of coil Δr	16	mm
			number of turns N_t	1250	–
			filling coefficient κ	0.785	
			permeability μ_r	1	–
			thermal conductivity (*) λ_T	306.1	W/m /°C
			electrical conductivity (*) γ_{el}	4.474×10^7	S/m
2	dilat. element	carbon steel ČSN 12 040 [4]	characteristic $B(H)$	Fig. 5	
			thermal conductivity (*) λ_T	Fig. 6	
			electrical conductivity (*) γ_{el}	4.5×10^6	S/m
			Young modulus E	2.1×10^{11}	N/m^2
			Poisson number ν	0.3	–
			coef. of thermal dilatation α_T	1.25×10^{-5}	1/ °C
3	plunger	Al	electrical conductivity (*) γ_{el}	3.5×10^7	S/m
			permeability μ_r	1	–
12 15	elements of the actuator (Fig. 2)	kevlar (TVA-RON)	thermal conductivity (*) λ_T	0.04	W/m /°C
			Young modulus E	1.24×10^{11}	N/m^2
			Poisson number ν	0.3	–
			coef. of thermal dilatation α_T	2×10^{-6}	1/ °C
18	thermally insulating shell (Fig. 2)	asbestos [6]	permeability μ_r	1	–
			thermal conductivity (*) λ_T	0.1–0.3	W/m /°C
			permeability μ_r	1	–
4 9 13 14 16 17	elements of the actuator (Fig. 2)	teflon [7]	permeability μ_r	1	–
			thermal conductivity (*) λ_T	1.6	W/m /°C

(*) modified with respect to the coefficient of filling

(**) unmovable air in the air gap, influence of convection neglected

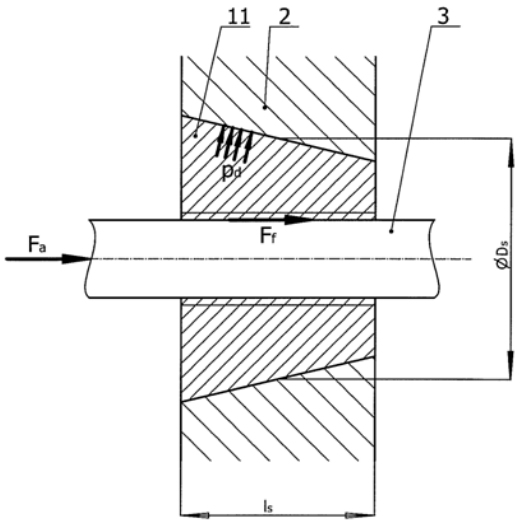

*Fig. 4b: Friction clutch $\mathbf{S}_2$: **2** – dilatation element of the thermoelastic actuator, **3** – plunger of the thermoelastic actuator, **11** – conical body of clutch $\mathbf{S}_2$*

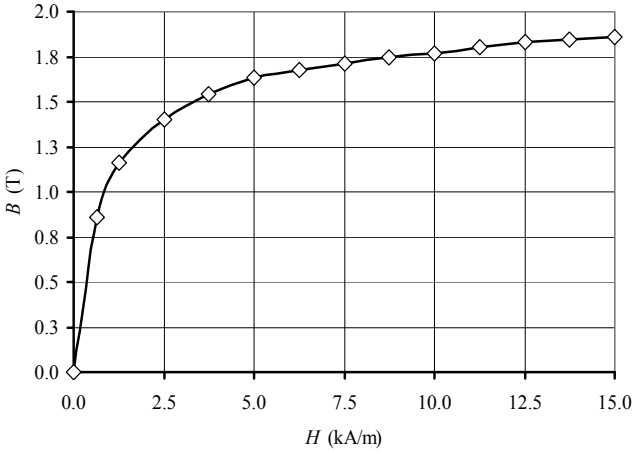

Fig. 5: Dependence B(H) of steel CSN 12 040 (see [4])

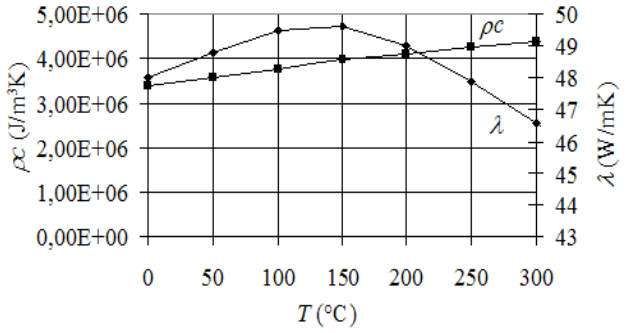

Fig. 6: Dependencies $\lambda = \lambda(T)$ and $\rho c = \rho c(T)$ for carbon steel 12 040

After formulating the mathematical model of the thermoelastic actuator (see [3]) that consists of three partial differential equations (PDEs) describing the electromagnetic field, temperature field and field of thermoelastic displacements and other structural parts (auxiliary actuators and self-locking friction clutches) it is possible to realize the discretized model whose numerical solution provides the operation characteristics of all basic components of the device.

Tab. 2: Physical parameters of the basic elements of the auxiliary actuators $\mathbf{A}_1$ *and* $\mathbf{A}_2$ *(see Figs. 3a, 3b)*

	element	material	parameter	value	dim.
$\mathbf{c}_{11}$, $\mathbf{c}_{12}$	field coils actuator $\mathbf{A}_1$	Cu conductor	diameter of conductor D_c length of coil Δz thickness of coil Δr number of turns N_t filling coefficient κ permeability μ_r	1 12 5 60 0.785 1	mm mm mm – –
$\mathbf{c}_{21}$, $\mathbf{c}_{22}$	field coils actuator $\mathbf{A}_2$	Cu conductor	diameter of conductor D_c length of coil Δz thickness of coil Δr number of turns N_t filling coefficient κ permeability μ_r	1 14 5 60 0.785 1	mm mm mm – –
3	plunger	Al	electrical conductivity γ_{el} permeability μ_r	3.5×10^7 1	S/m –
5 **10**	ferromagn. hollow core ferromagn. full core	carbon steel ČSN 12 040 [4]	characteristic $B(H)$ thermal conductivity λ_T Young modulus E Poisson number ν coef. of thermal dilatation α_T	Fig. 5 Fig. 6 2.1×10^{11} 0.3 1.25×10^{-5}	 N/m^2 – 1/ °C
6	nonferro-magnetic body of the friction clutch	Al	see **3,** Fig. 4b		

2 OPERATION CHARACTERISTICS OF SELECTED ELEMENTS OF THE DEVICE

The thermoelastic actuator

For an illustration, we present static characteristics of the most important elements of the device in Fig. 2. Fig. 7 shows the distribution of the specific Joule losses p_J in the dilatation element **2** in the dependence on the field current density J_{ext} in the field coil **1** when its frequency $f = 50$ Hz. This dependence is slightly nonlinear, but it allows full controlling of these losses representing the sources of heat for the consequent nonstationary temperature field in interval $(5-25)\times10^6$ W/m^3, while the field current density changes in interval $(1-2)\times10^7$ A/m^2.

Fig. 8 shows the evolution of the average temperature T_a of the dilatation element **2** in time t, as a function of the field current density J_{ext} for frequency $f = 50$ Hz. It is obvious that the temperature T_a may also easily be controlled (in interval $90-280$ °C) when the field current density changes in interval $(1-2)\times10^7$ A/m^2, within about 60 s. On the other hand, the value of T_a may easily exceed the temperature acceptable from the viewpoint of insulation of the field coil **1** (in our case 200 °C).

Tab. 3: Physical parameters of the basic elements of the friction clutches $\mathbf{S}_1$ *and* $\mathbf{S}_2$ *(see Figs. 4a, 4b)*

	element	material	parameter	value	dim.
2	dilat. element	carbon steel ČSN 12 040 [4]	characteristic $B(H)$ thermal conductivity λ_T electrical conductivity γ_{el}	Fig. 5 Fig. 6 4.5×10^6	 S/m
			Young modulus E Poisson number ν coef. of thermal dilatation α_T	2.1×10^{11} 0.3 1.25×10^{-5}	N/m^2 – 1/ °C
3	plunger	Al	electrical conductivity γ_{el} permeability $\mu_{r\,r}$	3.5×10^7 1	S/m –
6	conical sleeve of friction clutch $\mathbf{S_1}$	carbon steel ČSN 12 040 [4]	see **7**, Fig. 4a		
7	conical body of friction clutch $\mathbf{S_1}$	Al	see **3**, Fig. 4a		
11	conical body of friction clutch $\mathbf{S_2}$	Al	see **11**, Fig. 4b		

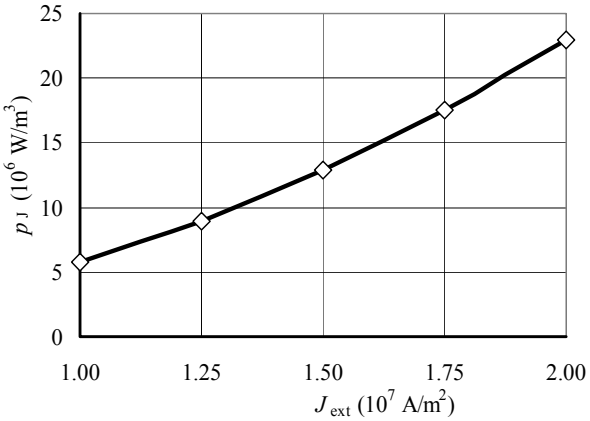

Fig. 7: Dependence of specific Joule losses p_J *in dilatation element* **2** *on the field current density* J_{ext} *in field coil* **1** ($f = 50$ Hz)

Figure 9 depicts the distribution of the maximum thermoelastic displacement $u_{z,max}$ of the dilatation element **2** in time t as a function of field current density J_{ext} in coil

1 (for frequency $f = 50$ Hz). It is clear that the corresponding shifts may be regulated in a relatively wide interval $(15-60)\times10^{-5}$ m by current $J_{\text{ext}} \in \langle 1-2\rangle \times 10^7$ A/m^2 within about 60 s. But even here some of the dilatations may be physically unreal due to unacceptable temperatures (see the discussion to Fig. 8).

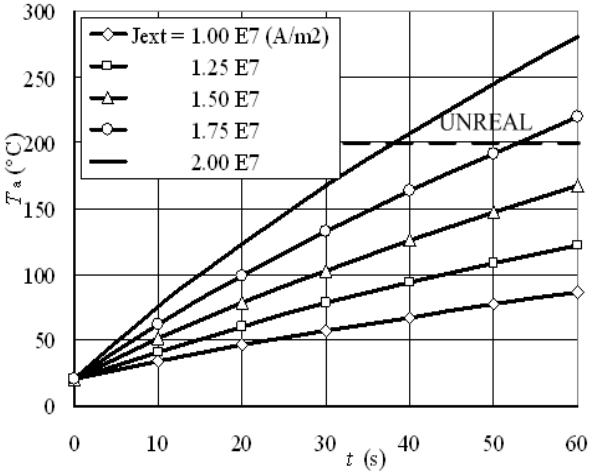

*Fig. 8: Distribution of the average temperature T_a of the dilatation element **2** in time t as a function of field current density J_{ext} (for $f = 50$ Hz)*

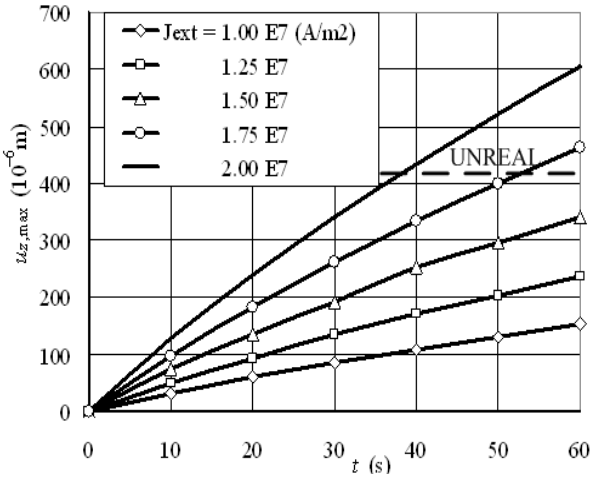

*Fig. 9: Distribution of maximum thermoelastic displacement $u_{z,\max}$ of the dilatation element **2** in time t as a function of field current density J_{ext} (for $f = 50$ Hz)*

Fig. 10 contains the time evolution of maximum values of reduced stress $\sigma_{\text{red,max}}$ of the dilatation element **2** according to the van Mise hypothesis (see, for example, [8]) as a function of J_{ext} in the field coil **1** for frequency $f = 50$ Hz. For steel CSN 12 040 used for the dilatation element the yield stress $\sigma_{\text{K}} = 300$ MPa (see, for example, [9]), and this value is not exceeded in our case. But similarly as in previous cases, unacceptable can become the temperature (see discussions to Figs. 8 and 9).

The auxiliary actuators $\mathbf{A}_1$ *and* $\mathbf{A}_2$

The operation characteristics of auxiliary actuators $\mathbf{A}_1$ and $\mathbf{A}_2$ (Figs. 3a and 3b) are presented in Figs. 11, 12, and 13. Fig. 11 depicts the static characteristic of actuator $\mathbf{A}_1$ and Fig. 12 an analogous characteristic for $\mathbf{A}_2$. It is clear that the forces $F_{\text{m},z}$ generated by the actuators:

- Strongly depend on the field current density J_{ext} (for $J_{\text{ext}} \in \langle 1-2\rangle \times 10^7$ A/m^2 these forces lie in interval $\langle 0,400\rangle$ N),
- Depend also on the position of the ferromagnetic hollow core **5** of the actuators with respect to their field coils $\mathbf{c}_{11}\ldots\ \mathbf{c}_{22}$ (coordinate ξ, see Figs. 3a and 3b). This dependence exhibits an extreme, i.e., there exist an optimum position ξ_{opt} for which the force $F_{\text{m},z}$ reaches its maximum (at a given J_{ext}).

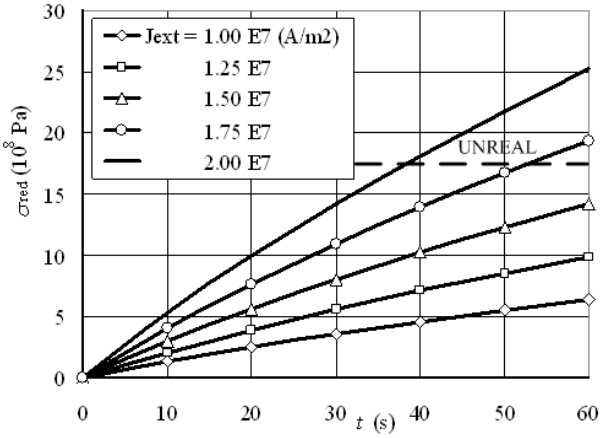

*Fig. 10: Distribution of the reduced stress σ_{red} (according to the van Mise hypothesis) of the dilatation element **2** in time t as a function of field current density J_{ext} (for $f = 50$ Hz)*

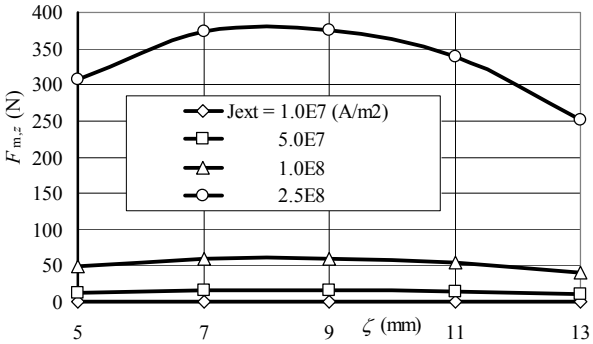

Fig. 11: Static characteristic of actuator $\mathbf{A}_1$

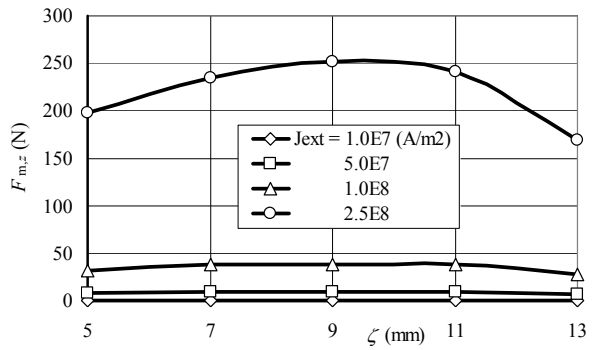

Fig. 12: Static characteristic of actuator $\mathbf{A}_2$

Figure 13 depict the maximum forces $F_{m,z,max}$ that may be generated by both actuators $\mathbf{A}_1$ and $\mathbf{A}_2$ at a given value of the field current density J_{ext}.

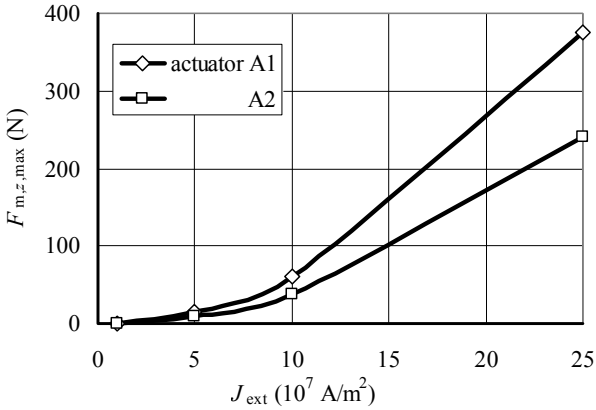

Fig. 13: Maximum forces $F_{m,z,max}$ of actuators $\mathbf{A}_1$ and $\mathbf{A}_2$ as functions of field current density J_{ext}

The self-locking friction clutches $\mathbf{S}_1$ and $\mathbf{S}_2$

The operation characteristics of clutches $\mathbf{S}_1$ and $\mathbf{S}_2$ are shown in Figs. 14, 15, and 16. Figures 14 and 15 show the dependencies of the pressure p_d over the conical surfaces of the clutches on the axial force $F_a \approx F_{m,z}$ generated by actuators $\mathbf{A}_1$ and $\mathbf{A}_2$. As the maximum acceptable pressure for both clutches $p_{d,max} \in \langle 0.3 - 5.0 \rangle$ MPa [11], it is clear that both of them can transfer even much higher forces than we consider. From the viewpoint of suitability, it is better to use clutches of greater lengths l_s and greater angle of conicity α.

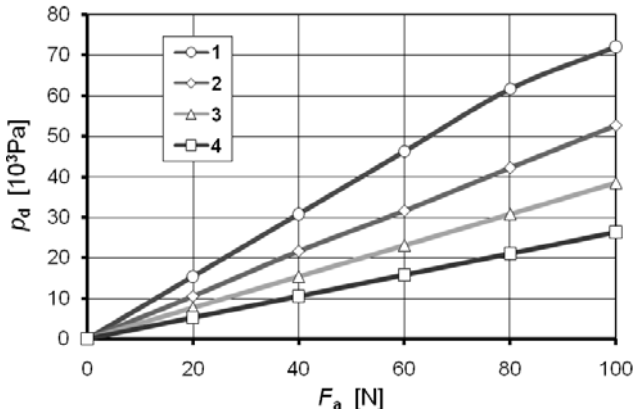

Fig. 14: Dependence of pressure p_d in the conical surface of clutch $\mathbf{S}_1$ on force F_a generated by actuator $\mathbf{A}_1$
1 – $l_s = 20$ mm, $\alpha = 15°$, **2** – $l_s = 20$ mm, $\alpha = 30°$,
3 – $l_s = 40$ mm, $\alpha = 15°$, **4** – $l_s = 40$ mm, $\alpha = 30°$

Finally, Fig. 16 shows the dependence of the friction force F_f between the plunger **3** and internal cylindrical surface of the conical body **7** of the friction clutch $\mathbf{S}_1$ on the axial force F_a generated by actuators $\mathbf{A}_1$ and $\mathbf{A}_2$. It is obvious that from the viewpoint of this force smaller angles α are better.

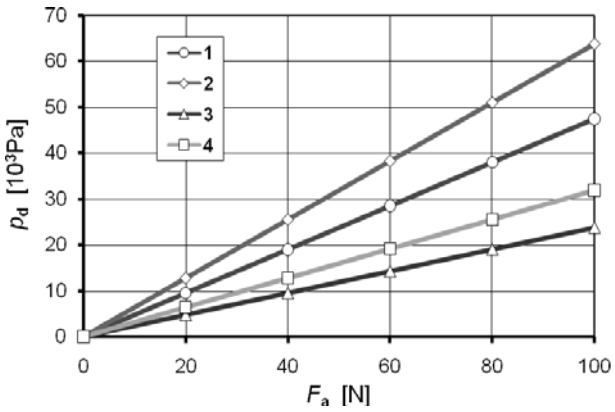

Fig. 15: Dependence of pressure p_d in the conical surface of clutch $\mathbf{S}_2$ on force F_a generated by actuator $\mathbf{A}_2$
1 – $l_s = 20$ mm, $\alpha = 15°$, **2** – $l_s = 20$ mm, $\alpha = 30°$,
3 – $l_s = 40$ mm, $\alpha = 15°$, **4** – $l_s = 40$ mm, $\alpha = 30°$

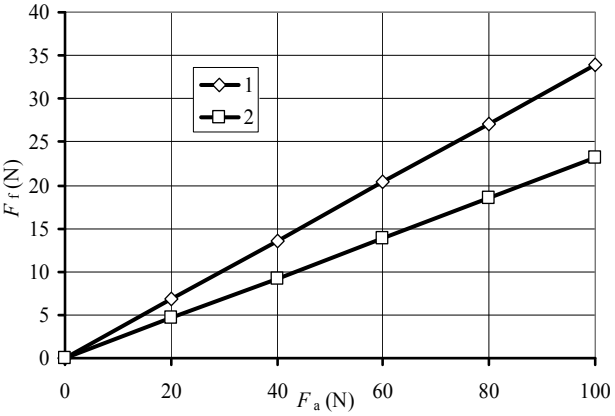

Fig. 16: Dependence of the friction force F_f in clutch $\mathbf{S}_1$ on the axial force F_a generated by actuator $\mathbf{A}_1$
line **1** – $\alpha = 15°$, *line* **2** – $\alpha = 30°$

3 CONCLUSION

A more detailed description of the considered controllable actuator and its characteristics may be found in [3]. But its complete description and its technological employment is presented on www pages http://147.228.94.30/ of the Czech electronical journal Electroscope.

REFERENCES

[1] Doležel, I., Karban, P., Ulrych, B., Pantelyat, M., Matyukin, Y., Gontarowskiy, P.: Numerical Model of a Thermoelastic Actuator Solved as a Coupled Contact Problem. COMPEL, Vol. 26, 2007, No. 4, pp.1063–1072.

[2] Pantelyat, M., Matyukin, Y, Gontarowskiy, P., Doležel, I., Ulrych, B.: Computer Simulation of Actuators Working on Principle of Thermoelasticity. Proc. ICEM 2006, 2–5. 09. 06. Chania, Greece. Book of Abstracts, pp. 272.

[3] Doležel, I., Krónerová, E., Ulrych, B.: Induction Thermoelastic Actuator with Controllable Operation Regime. ISEF 2009 - XIV International Symposium

on Electromagnetic Fields, Arras, France, September 2009, accepted.
[4] Company standard SKODA 00 6004 (in Czech).
[5] www.azom.com (June 2009)
[6] Mikulčák, J. et al: Mathematical, Physical and Chemical Tables (in Czech). SPN Praha, 1970.
[7] Hassdenteufel, J., Květ, K. et al: Materials for Electrical Engineering (in Czech). SNTL Praha, 1967.
[8] Černoch, S.: Tables for Technical and Mechanical Engineering (in Czech). SNTL Praha, 1977.
[9] http://www.vitkovicesteel.com/produkty-detail/produkty/-1/produkty-podsekce/plechy-z-konstrukcnich-oceli-2/produkty-detail/plechy-z-oceli-podle-en-10025-2-2/ (July 2009).
[10] Hosnedl, S., Krátký, J.: Booklet of Mechanical Engineer 1, General machine parts (in Czech). Computer Press, Brno, 1999.
[11] www.diafrikt.cz.

Authors: Prof. Ing. Ivo Dolezel, CSc., Czech Technical University, Faculty of Electrical Engineering, Technicka 2, 166 27 Prague, CR, E-mail: dolezel@fel.cvut.cz; Ing. Vaclav Kotlan, PhD., Assoc. Prof. Ing. Bohus Ulrych, CSc., University of West Bohemia, Faculty of Electrical Engineering, Univerzitni 26, 306 14 Pilsen, CR, E-mail: {vkotlan, ulrych}@kte.zcu.cz